Empirical Validation of Building Energy Simulation Model Input Parameter for Multizone Commercial Building during the Cooling Season

Yoon, Y.[a,1], Jung, S. [a,1], Im, P. [a,*], Salonvaara, M.[a], Bhandari, M.[a], Kunwar, N.[a]

[a] Buildings and Transportation Science Division, Oak Ridge National Laboratory, Oak Ridge, TN 37830, USA

1 = These authors contributed equally to this work.

* = corresponding author details, imp1@ornl.gov (Im, P)

Abstract

This paper presents a critical advancement in Building Energy Modeling (BEM) through an empirical validation approach using a high-quality dataset from a multizone commercial office building in Oak Ridge, TN, USA. BEM is widely utilized in diverse construction applications, but its effectiveness relies on the accuracy of its predictions. The study focuses on empirical validation of input parameters in BEM, including building envelope data, infiltration modeling, and rooftop unit system performance curves. The validation of simulation input parameters leads to substantial improvements in the accuracy of simulation results. Notable both NMBE and cv(RMSE) values are reduced by 0.5% for indoor air temperature and 17% for indoor air relative humidity compared to the previous model. At the system level, both NMBE and cv(RMSE) values are reduced by 2% for fan energy consumption and 4% for cooling energy consumption, compared to the previous model. A literature review highlights a significant gap in empirical validation studies, which predominantly concentrate on either component-level or whole building validation. Furthermore, many studies employ simplified setups that may not faithfully represent the complexities of multizone commercial buildings. This paper distinguishes itself by emphasizing the critical importance of component-level input parameter validation. It underlines the need to validate data related to building envelope components and HVAC system performance curves, resulting in more accurate simulation outcomes. The utilization of actual multizone commercial building data enhances the study's practical relevance. In summary, this research underscores the pivotal role of input parameter validation in enhancing the accuracy and reliability of BEM.

Highlights

- The EnergyPlus simulation model input parameters have been empirically validated.
- Building envelope input parameters have been evaluated.
- Tracer gas and blower door tests have been performed to update infiltration model.
- The rooftop unit performance curve has been developed using field datasets.
- The simulation results are well-matched with field data at zonal- and system-level.

Keywords: Empirical validation, ASHRAE standard 140, EnergyPlus, Building energy modeling, Input parameter, Commercial building

Word count: 7,896 words excluding title, author names and affiliations, keywords, abbreviations, table/figure captions, acknowledgements and references.

Nomenclature

Abbreviations

BEM	Building energy modeling
HVAC	Heating, ventilation, and air conditioning
FRP	Flexible Research Platform
RTU	Rooftop unit
DX	Direct expansion
DOE	U.S. Department of Energy
NMBE	Normalized mean bias error
cv(RMSE)	Coefficient of the variation of the root mean square error
IPMVP	International Performance Measurement and Verification Protocol
FEMP	Federal Energy Management Program
M&V	Measurement and Verification
CMU	Concrete mortar unit
ACH	Air change per hour
CFT	Total cooling capacity function of temperature curve
CFF	Total cooling capacity function of flow fraction curve
EFF	Energy input ratio function of flow fraction curve
EFT	Energy input ratio function of temperature curve
PLF	Part load fraction correlation curve

W/m·K	Watts per meter-kelvin
m^3/s	Cubic meter per second
kg/m^3	Kilogram per cubic meter
h	Hour
Wh	Watt hour
J/kg	Joule per kilogram
W	Watt
kg/s	Kilogram per second

Symbol

R_{SI}	R-value of building material in SI unit
I_{design}	Flow per exterior surface area
F_{sch}	Infiltration schedule
T_{zone}	Indoor air temperature
T_{odb}	Outdoor air temperature
α	Constant coefficient
β	Coefficient of the indoor and outdoor temperature difference
γ	Coefficient of wind speed
δ	Coefficient for the square of wind speed
W_s	Wind speed

SAT	Supply air temperature	α_{bldg}	Urban/suburban terrain environment coefficients
SARH	Supply air relative humidity	U_H	Reference window speed
RAT	Return air temperature	ρ	Reference air density
RARH	Return air relative humidity, respectively	C_s	Average positive surface pressure coefficient on a wall due to wind effects
HF	Heat flux	n	Flow or pressure exponent
Mea	Measured	I_{75pa}	Air leakage at a pressure differential of 75Pa
Com	COMSOL results	Q	Airflow
Cav	Cavity	C	Flow coefficient
EPlus	EnergyPlus	ΔP	Pressure differential
Ext	Exterior surface temperature	C_i	Concentration in time i
In	Interior surface temperature	t	Sample time
		Power	Electric energy consumption of the cooling system
Units		$\dot{Q}_{total,rated}$	Rated total cooling capacity
W/m²·K	Watts per square-meter-kelvin	COP_{rated}	Coefficient of performance at rated conditions
m²·K/W	Square-meters-kelvin per watt	PLR	Part load ratio
kW	Kilowatt	WT	Entering web-bulb temperature
℃	Degree Celsius	DT	Dry-bulb temperature seen by condenser
%	Percentage	ff	Fraction of the full load flow
W/m²	Watts per square-meters	c	Coefficient for each curve
m	Meter	h_{ADP}	Enthalpy of air at the apparatus dew point condition
Pa	Pascal	h_{in}	Enthalpy of air entering the cooling coil
m/s	Meter per second	Q_{total}	Available cooling capacity
Deg	Degree	m	air mass flow rate
mm	Millimeter	BF	bypass factor

1. Introduction

1.1 Background

Building Energy Modeling (BEM) has been used as a critical tool to evaluate building energy savings potential for new and existing buildings for decades. More in detail, BEM has been extensively used in the field of building energy studies, such as for building performance evaluation [2]; lighting control [3-4]; heating, ventilation, and air conditioning (HVAC) system control [5-6]; building retrofits [7-8]; fault detection [9-10]; and predicted energy consumption [11-12]. Additionally, BEM is used for green certification, code compliance, and qualification for tax credits and utility incentives, as well as for or developing, revising, validating, and testing the building control algorithm before implementing it in real buildings.

However, it is often found that the modeled building energy performance is not consistent with the measured building performance, and the differences could be sometimes more than 30% [13]. In general, this discrepancy between the model and reality is mainly due to incorrect assumptions in model input values, inaccurate building model algorithm itself, uncertainty associated with real building operation [14]. Therefore, ensuring the accuracy and reliability of BEM has been a critical path to promote the use of BEM in building design and retrofit, which could increase the potential of energy and cost savings in buildings.

As an effort of validating BEM engines, ASHRAE published the ASHRAE Standard 140 in 2001, and it has been constantly updated [15]. The main purpose of the ASHRAE Standard 140 is to improve the accuracy of BEM engines by creating standardized test procedures for validation. ASHRAE Standard 140 defines three different approaches for validating the accuracy of BEM: the (1) comparative method, (2) analytic method, and (3) empirical validation method [16-18]. The comparative method does not need any actual data but does need simulation results from two or more BEM tools. Through this method, internal code can be improved by analyzing the differences among BEM tools. However, the comparative validation method cannot provide the ground truth data. The analytic method uses BEM, which is much simpler than using the actual building because of strictly controlled boundary conditions. The advantage of this method is that it helps identify existing issues in the internal code, especially in thermal solution algorithms (e.g., heat transfer). The disadvantage of this method, however, is that it has a limited number of configurations because of the strictly controlled boundary conditions. Since both the comparative method and the analytic method do not use real data, it is difficult to determine whether the performance of BEM is true to that of the actual building.

Unlike the comparative and analytic methods, the empirical validation method requires actual ground truth data from real buildings, enabling the comparison of simulation results with ground truth data. However, the empirical validation method requires much effort, including sensor and monitoring device installation and data gathering, to obtain measured datasets. Furthermore, because of uncertainties in building and occupancy conditions and scenarios, real buildings need to be operated with carefully designed condition to eliminate the associated uncertainties.

As a result of the difficulty of obtaining "validation-grade" empirical measurements for whole-building energy simulations, ASHRAE Standard 140 has historically relied on comparative and analytical tests. However, US national laboratories have built research facilities and now validation-grade experiments are possible with well-characterized, highly-instrumented test facilities like Oak Ridge National Laboratory's Flexible Research Platform (FRP) and Lawrence Berkeley National Laboratory's Facility for Low Energy eXperiments (FLEXLAB). With the intention of incorporating their results into the standard, DOE has continually funded validation experiments at these two facilities [15].

There were previous studies for the component-level empirical validation. Regarding the glazing and shading system, Loutzenhiser et al. conducted an empirical validation of solar gains through an insulating glazing unit. They developed BEMs, namely EnergyPlus, DOE-2.1E, TRNSYS, HELIOS, and ESP-r, among which the EnergyPlus model showed the highest prediction rate [19-21]. Meanwhile, Nouidui et al. used the Modelica building library [22] to compare simulated glass temperature with actual data and found that the temperature difference between measured and simulated data is high during the daytime because temperature sensors absorb solar radiation [23]. For the double skin façade (DSF) system, Lucchino et al. validated a DSF system model using the comparative method and the empirical validation

method [24]. Mateus et al. developed the EnergyPlus model and empirically validated the model using air temperature and radiant temperature in the DSF system [25]. Kalyanova et al. performed empirical validation of a DSF system through the TRNSYS, ESP-r, VA114, and BSim programs. For the empirical validation, they compared total solar radiation on the external DSF surface, heating and cooling energy consumption, and air temperature and mass flow rate in the DSF cavity [26]. For the exterior wall, Kuznik et al. conducted validation of the exterior wall with phase change material (PCM) through the TRNSYS program. They compared the interior and exterior surface temperature of the exterior wall [27]. Also, Buonomano and Guarino validated the PCM wallboards using the DETECt tool [28]. They used field data to evaluate multiple modeling approaches (3 heat curves, 4 hysteresis models) for accurate temperature-dependent heat capacity curve selection in PCM performance analysis [28]. Herrando et al conducted experimental validation of the hybrid photovoltaic-thermal (PVT) collectors and heat pump [29]. They compared outlet temperature of PVT collectors, electric energy consumption of PVT collectors, thermal efficiency of PVT collectors, and district hot water temperature [29].

For the empirical validation for whole building model, Cattarin et al. validated BEMs using both the comparative method and the empirical validation method. They conducted a field test at a test cell located in France and developed both Matlab and TRNSYS models. They used indoor air temperature, radiant temperature, envelope's (exterior wall, floor, and glazing) internal surface temperature [30]. Eguía-Oller et al. empirically validated a TRNSYS model using actual data of the twin house. They developed the TRNSYS model with an airflow network function to validate indoor air temperature in each room and heating energy consumption [31]. Nageler et al. developed and validated 1D BEM tools which are Dymola, EnergyPlus, TRNSYS, and IDA ICE models. The research focused on the evaluation of the performance of 1D BEM tools against 3D CFD (ANSYS Fluent simulations) and actual data from a real test box. For empirical validation purposes, they used indoor air temperature, ceiling surface temperature, concrete temperature, and return water temperature [32]. Barone et al. validated the Matlab model with the actual data from the test room. To empirically validate the Matlab model, indoor air temperature, outdoor air temperature, mean radiant temperature, exterior wall, ceiling, and floor surface temperature, and heating and cooling demand were used [33]. Strachan et al. conducted whole model empirical validation using two full-scale buildings. 21 modelling team used commercial and research simulation programs including, eQuest, Matlab, TRNSYS, ESP-r, Modelica, and EnergyPlus. For this exercise, they used indoor air temperature and heating demand [34].

The literature review reveals a significant gap in the existing empirical validation studies related to building energy modeling. Previous research has primarily focused on either detailed component-level validation (e.g., building envelop component, equipment, etc.) [19-21 and 23-29] or whole building energy modeling validation [30-34], with limited attention to comprehensive validations that encompass both aspects. This gap is critical because neglecting component-level validation can lead to inaccuracies in building component models and subsequently impact indoor thermal conditions. Furthermore, most empirical validation studies have utilized simplified setups such as one-zone test chambers [19-21, 23-28, 30, and 32-33] or single-family houses [31 and 34], which may not adequately represent the complexities of multizone commercial buildings commonly found in the real world.

The primary goal of this paper is to address these knowledge gaps and contribute to the field by demonstrating the importance of component-level input parameter validation in influencing both whole building indoor conditions and energy consumption.

The novelty of this research lies in its comprehensive approach, as it not only emphasizes the significance of component-level input parameters validation but also provides practical solutions for the validation.

- Comprehensive Component-Level Validation: Unlike many previous studies that have primarily focused on whole building-level validation, this research places a strong emphasis on the validation of component-level input parameters. It demonstrates the importance of validating data related to building envelope components, such as exterior wall, roof, and glazing properties, as well as heat transfer characteristics. This comprehensive approach ensures that the building's fundamental components are accurately represented in the simulation model, leading to more reliable simulation results.
- HVAC System Performance Curve Development: The research also addresses another critical aspect often overlooked in previous studies - the validation of HVAC system performance curves. Instead of relying on generic cooling performance curves, the paper demonstrates how to develop specific performance curves using measured HVAC performance data and implement them within the EnergyPlus simulation program. This is a significant contribution as it ensures that simulations are representative of the actual installed HVAC systems in test buildings.
- Actual Multizone Commercial Building Data: To enhance the relevance and applicability of the study, this paper uses high-quality and high-resolution datasets from full-scale multizone commercial buildings.

In summary, this paper's goals are not only novel but also highly relevant in advancing the field of building energy modeling. This paper does not primarily focus on validating the building energy simulation engine but rather on validating the input parameters of the simulation model. This study emphasizes the importance of input parameter validation in the context of building energy simulation model validation. It aims to elucidate the crucial role that simulation model input parameter validation plays in ensuring the accuracy and reliability of building energy simulations.

1.2 Objectives

This paper is an update of the previous publication [1], which outlines detailed model validation efforts with promising validation results in the building energy end use analysis. The paper described several future works to improve the model input parameters to provide better description of the model. For example, as shown in Figure 1, the EnergyPlus model developed by the model input parameters presents that there are some discrepancies between modeled and simulated room air temperatures although the measured and simulated energy use showed pretty good match. To improve the validation of the model, the authors suggested to perform further component-level validation using the detailed measured dataset. Also, improving the HVAC system performance curve based on actual data would be recommended.

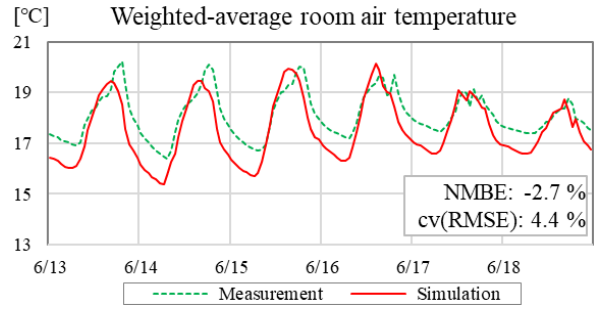

(a) Weighted-average room air temperature comparison for test 1.

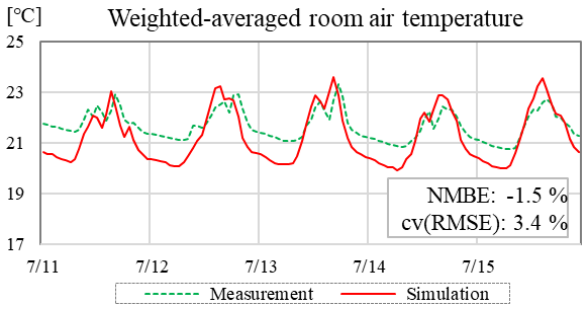

(b) Weighted-average room air temperature comparison for test 2.

Figure 1. Weighted-average room air temperature comparison in Im et al.'s 2020 study.

Figure 2 shows the overall framework of this paper. The main objective of this study is to provide an updated input document (i.e., thermal properties of the building envelope and HVAC system performance curve) and field dataset (i.e., energy consumption and indoor and outdoor conditions). To update the input document and field dataset, additional experimental studies have been performed, which include the following:

- validation of building envelope component, including exterior wall, roof, and window;
- further test and modeling to improve the building and zonal infiltration model;
- RTU performance curve improvement to model latent load correctly; and
- reconducting the cooling season baseline test.

In this paper, which is an update to our previous publication [1], we have made various efforts to enhance the validation of the simulation model while highlighting the distinctions from our earlier work. Our current study places particular emphasis on validating building envelope components, retesting the building and zonal infiltration model, and regenerating the RTU performance curve using field data.

Regarding system operation, our previous study exclusively enabled the central packaged cooling coil during tests, without incorporating a zonal reheating coil [1]. This setup led to fluctuating zonal temperatures, as depicted in Figure 1. In contrast, in the current study, both the central packaged cooling coil and zonal reheating coils were activated to better replicate realistic building operation.

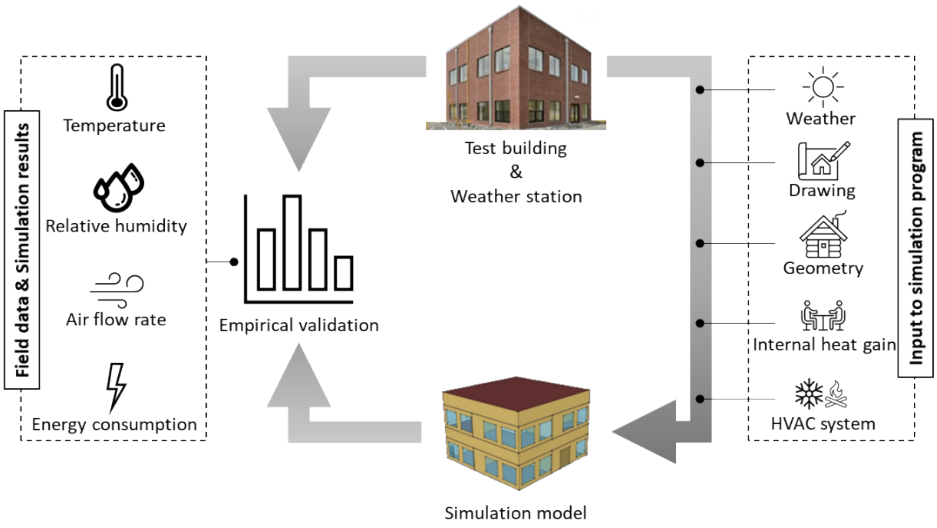

Figure 2. Overall framework of the research.

This paper contains six main sections. Section 1 is introduction and literature review. Section 2 contains information about the test building. Section 3 addresses the methodology used in this study and Section 4 focuses on input value development for the simulation model. Section 5 shows the main results of this study. Throughout the whole study, the EnergyPlus model developed per the model input parameters has been used. This study does not attempt to validate EnergyPlus engine, but rather use the EnergyPlus engine to evaluate the accuracy of the model input parameters. Two other models from different simulation engines were also used to serve the same purpose, but this paper does not cover the results. Conclusion and future work are described in Section 6.

2. Test bed

2.1 Test building

The ORNL's FRP building is selected as the test building for this study. The FRP is a two-story building with 13.4 m width and depth, as shown in Figure 3. Each floor has five conditioned zones and an unconditioned staircase. Floor to floor height of the first floor is 4.1 m, and floor to ceiling height of the first floor is 2.7 m. For the second floor, floor to floor height is 4.2 m, and floor to ceiling height is 2.4 m. Table 1 shows the building geometry information. The window to wall ratio of the FRP building is 28%. For the internal heat gain, lighting power density is 9.18 W/m^2 and equipment power density is 14.04 W/m^2. However, for this study, lighting and equipment were turned off to reduce the uncertainty associated with the lighting and plug loads.

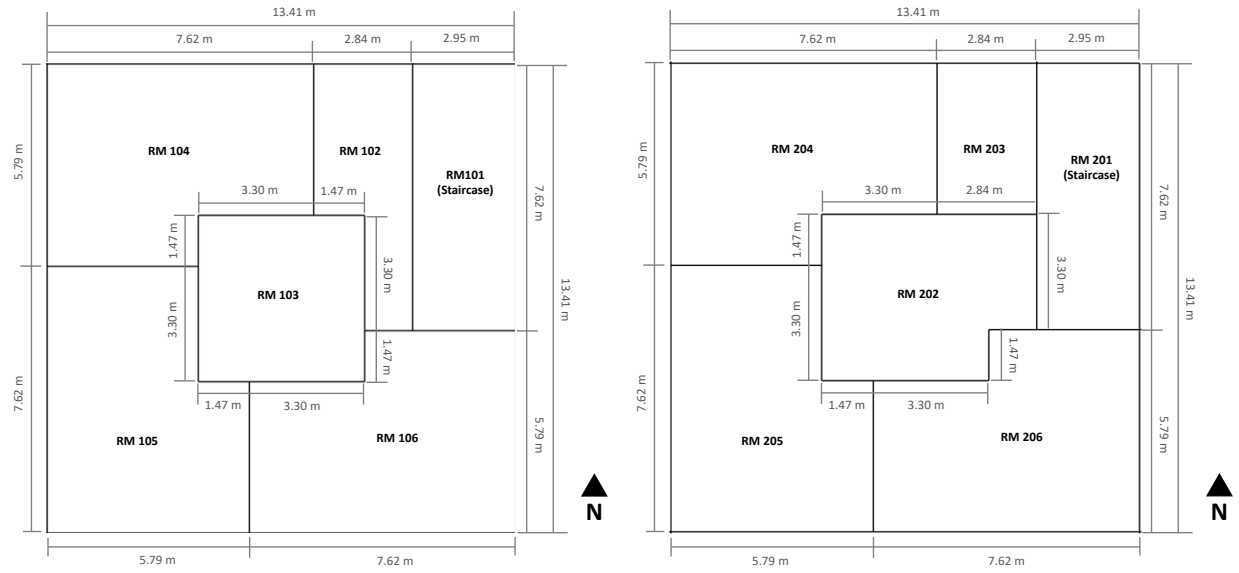

(a) First floor plan

(b) Second floor plan

Figure 3. Floor plan of the FRP building.

Table 1. Building geometry information.

Construction	Information	U-value ($W/m^2 \cdot K$)
Wall	Concrete masonry units with fiberglass R_{SI}-1.9 ($m^2 \cdot K/W$) and face brick	0.363
Floor	Slab on grade	0.104
Roof	Metal deck with polyisocyanurate (R_{SI}-3.17) and ethylene propylene diene monomer	0.311
Windows	Double-pane clear glazing with aluminum frame	2.76

2.2 HVAC systems

The RTU with DX cooling coil is served as main cooling system for the FRP building. The RTU has variable frequency drive supply fan to modulate the total air flow to the zones, and the supply air flow is modulated to maintain the static pressure setpoint in the main duct. Each zone in the FRP has variable air volume (VAV) box with electric reheating coil. Each VAV box has a damper to modulate the zonal air flow, and reheating is engaged when the zone temperature is below the heating setpoint. The capacity of the RTU is 44 kW (12.5 ton) with a 9.6 energy efficiency rating.

2.3 Sensor and data monitoring

More than 500 sensors—including zone temperature and relative humidity, supply and return air temperatures, relative humidity, airflow rate, and power measurements—were installed in the FRP

building. The field data were collected by the data logger and the building automation system installed in the FRP building. Figure 4 shows the sensor types and locations in the HVAC system. Table 2 shows the installed sensor accuracy.

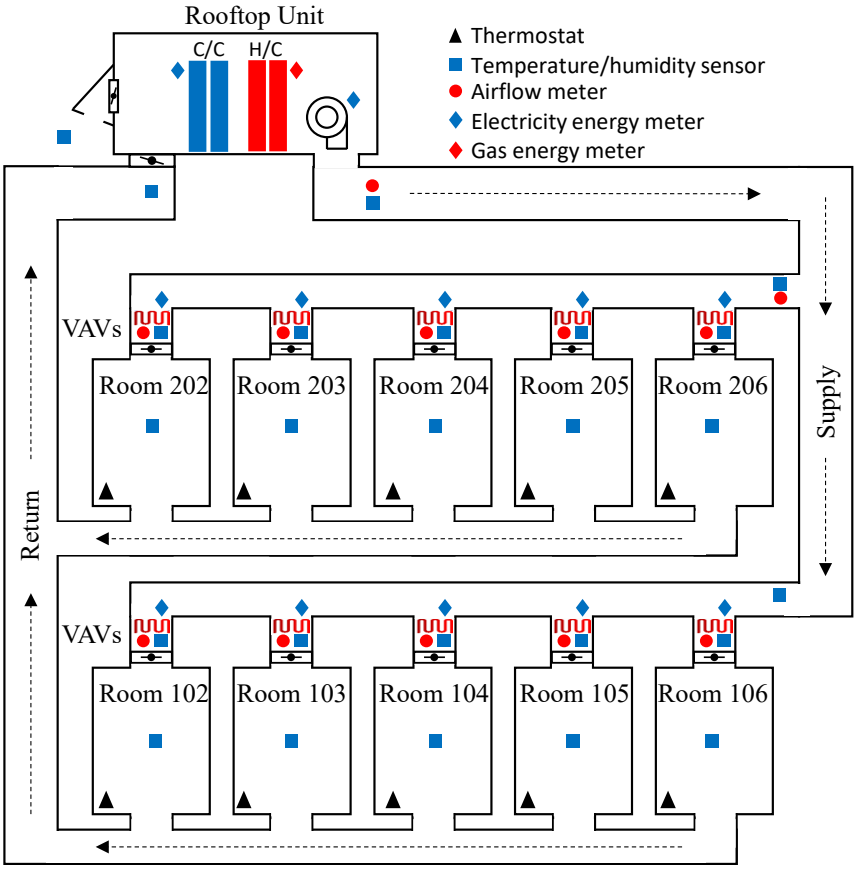

Figure 4 . HVAC system and current measurements of the FRP building.

Table 2. Installed sensor accuracy.

Sensors	Measurement	Accuracy	Reference
Campbell Sci HC2S3-L	Temperature Relative humidity	±0.1°C for temperature ±0.8% at 23°C for relative humidity	[35]
Continental Controls WNB-3D-240P	Power	±0.5% of reading	[36]
Omega PX409-750-A5V pressure transducers	Pressure	±0.08% best straight-line maximum	[37]
Air Monitor fan evaluators paired to DPT 2500-plus transmitters	Air flow	0.25% of natural span Fan evaluator - ±2%	[38]

Heat flux sensor (FHF02)	Heat flux	± 5 %	[39]

2.4 Weather station

Figure 5 shows the dedicated weather station installed on the roof of the FRP building. Weather data was collected every 30 seconds, and the variables and units collected are shown in Table 3. The weather data was used to pack the actual meteorological year weather file to be used for the simulation.

Figure 5. Weather station.

Table 3. Weather data variables and units.

Sensor type	Instruments	Description	Units
Solar radiation	Eppley SPP	Global solar radiation	W/m^2
	Eppley sNIP	Direct solar radiation	W/m^2
	Eppley Model 8-48	Diffuse solar radiation	W/m^2
Air property	Campbell Sci HC2S3-L	Outdoor air temperature	℃
		Outdoor air humidity	%
	Vaisala- CS106	Barometric pressure	Pa
Wind	Young Wind Monitor Model 05103	Wind speed	m/s
		Wind direction	Deg

3. Methodology

3.1 Experimental study

To validate the model input parameters, experimental studies were carried out. The cooling season test was performed from July 8–14, 2021. The test conditions were as follows:

- Windows and doors were closed.
- Window blinds were not used.
- No internal heat gain during the test period.
- The discharged air temperature was fixed as 12.8℃.
- 100% of the indoor air was returned to the HVAC system (no outdoor air intake).
- Static pressure was fixed as 249 Pa.
- The cooling setpoint temperature was maintained at 24℃ without a setback temperature setting.
- The main heating system (gas furnace) was turned off, and the VAV reheating was turned on.

The detailed information regarding the test facility has been comprehensively described in our previous publication [1 and 40]. Additionally, the field data used in this study is publicly accessible [41] and has been validated in the previous publication [40].

3.2 Simulation study

OpenStudio SketchUp plug-in was used for the building geometry modeling. DOE's EnergyPlus whole building energy program was used for detailed simulation modeling and HVAC system modeling. The EnergyPlus simulation model was developed based on the experimental data. Figure 6 shows the FRP building and the rendering of EnergyPlus simulation model.

(a) Test building (b) Rendering of simulation model

Figure 6. Test building and simulation model.

To achieve the goal of this study, the initial simulation model [1] was revised based on further investigation and tests, particularly in the three aspects below.

- Building envelope components
- Building infiltration model
- Performance curve for cooling system

3.3 Simulation model validation

To improve the accuracy of model input parameters, two metrics were used; NMBE and cv(RMSE). ASHRAE Guideline 14-2014, the International Performance Measurement and Verification Protocol (IPMVP), and the Federal Energy Management Program (FEMP) are representative measurement and verification (M&V) guides, and these M&V guides provided the tolerance range of cv(RMSE) and NMBE. Although this study is not attempting calibration of the model, the same metric was used to evaluate the accuracy of the model input parameters. Table 4 shows the tolerance range indicated in each M&V guide [42-44]. The allowable error rate of the tolerance range varies depending on the M&V guide.

Table 4. Tolerance range in each M&V guide.

Data interval		**Tolerance range**		
		ASHRAE Guideline 14-2014 (%)	FEMP (%)	IPMVP (%)
Monthly	NMBE	±5	±5	± 20
	cv(RMSE)	15	15	-
Hourly	NMBE	±10	±10	± 5
	cv(RMSE)	30	30	20

4. Simulation model development

4.1 Weather data generation

Accurate weather input information is one of the most important factors in input parameter validation. We collected weather data including dry-bulb temperature, relative humidity, global, direct normal and diffuse solar radiation, and wind speed and directions from the weather station at the roof of the test building. Then, the EnergyPlus weather file (.EPW) was packed using the measured data to be used for the simulation.

4.2 Building opaque envelope component development

4.2.1 Simulation tool

COMSOL Multiphysics [45] is a general-purpose finite element analysis, solver, and multiphysics simulation software. The tool allows for single-physics and fully coupled multiphysics modeling with advanced numerical methods to simulate real-world designs, devices, and processes. EnergyPlus models the walls in one dimension only. We used COMSOL to model the assembly as built in 2D and validated the details of the structure (e.g., thermal conductivities and thermal capacity) with COMSOL. COMSOL also provided us then the effective one-dimensional structure that produces the same heat flux over the whole wall surface as the two-dimensional assembly.

4.2.2 Exterior wall evaluation

The evaluated wall construction, shown in Figure 7, has the following layers as per the architectural drawings starting from the exterior: 92 mm full brick cladding, 25 mm air space, 203 mm concrete mortar

unit (CMU), 89 mm fiberglass cavity insulation with 63.5 mm steel frame (with 25.4 mm air gap), and 12.7 mm interior gypsum drywall.

The evaluation process uses 2D simulations to predict the measured temperatures and heat fluxes as a function of time. Once the simulated and measured heat fluxes agree, the 2D layers will be simplified by creating effective 1D material properties for a homogeneous layer that produces the same transient and steady-state response as the simulation of the 2D structure. The 1D structure and material properties are subsequently used to model the wall in the EnergyPlus simulation program.

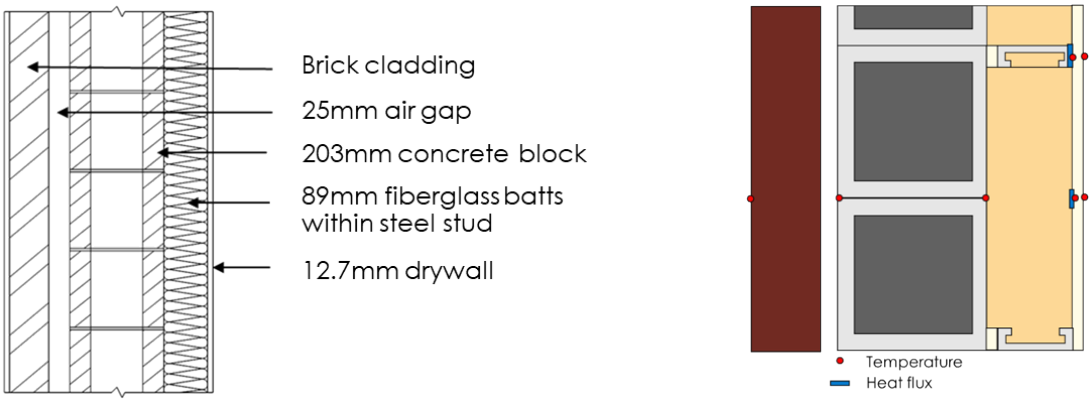

(a) Vertical layout of the wall structure in the drawing

(b) Sensor location

Figure 7. Wall structure and sensor location.

4.2.3 Exterior wall development

A horizontal section of the wall assembly is presented in Figure 8. Figure 8(a) shows the horizontal layout of the wall structure as modeled in COMSOL. "HfmeasCavity" in Figure 8(a) indicates the location where the heat flux on the center of the stud was measured, and "HfmeasStud" in Figure 8(a) indicates the location where the heat flux on stud was measured. Red lines in Figure 8(b) indicate the boundaries of the layers that need conversion to homogeneous 1D properties for EnergyPlus modeling (CMU block and the insulated cavity with steel stud).

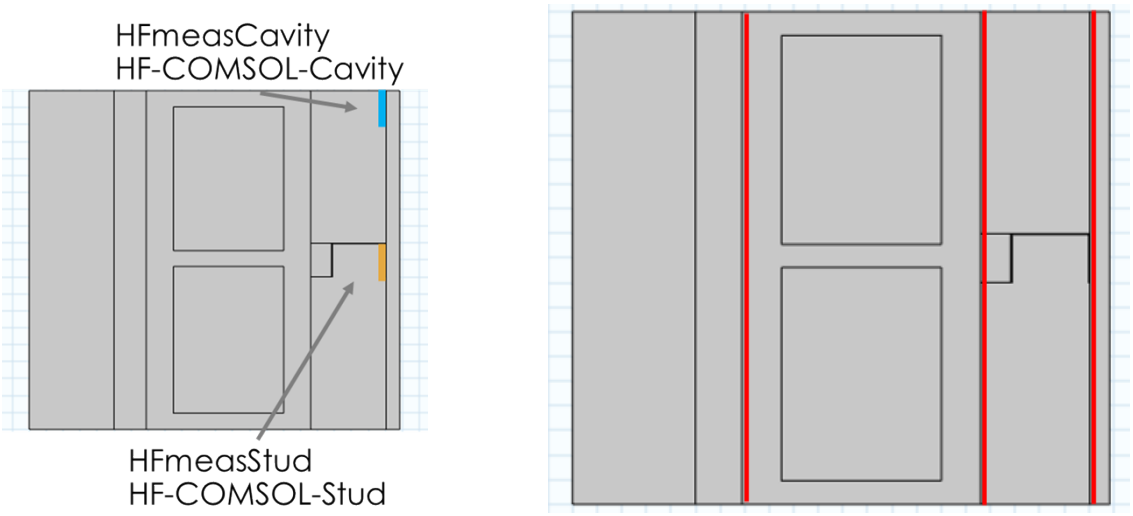

(a) Horizontal layout of the wall structure in COMSOL

(b) Horizontal layout of the wall structure in EnergyPlus

Figure 8. Horizontal section of the wall assembly.

First, the properties of the materials in the COMSOL [45] simulations were adjusted so that the measured and simulated heat fluxes matched when using the measured surface temperatures as boundary conditions. A steady-state simulation was carried out with COMSOL to calculate the overall U-value of the structure. Then, the layers with 2D details, the CMU block and the insulated cavity with a steel stud, were assigned a 1D material with a thermal conductivity so that the resulting U-value was the same. Finally, volume averaging of the individual materials in the converted layers produced the thermal capacity of the 1D layers. The overall R-value of the wall structure changed from the initially used 1.532 to 2.607 $m^2 \cdot K/W$. Figure 9(a) shows the measured and simulated heat fluxes at the locations as shown in Figure 8(a), and Figure 9(b) and (c) compare the measured and EnergyPlus simulated surface temperatures. “HF,” “Mea,” Com,” and “Cav” in Figure 9(a) indicate heat flux, measured data, COMSOL results, and cavity, respectively. “EPlus,” “Ext,” and “In” in Figure 9 (b) and (c) indicate EnergyPlus simulation results, exterior surface temperature, and interior surface temperature, respectively. The NMBE for the exterior and interior surface temperatures is 6.8% and 6.5%, respectively, and the cv(RMSE) for the exterior and interior surface temperatures is 7.1% and 8.0%, respectively. Both NMBE and cv(RMSE) values are in the acceptable range.

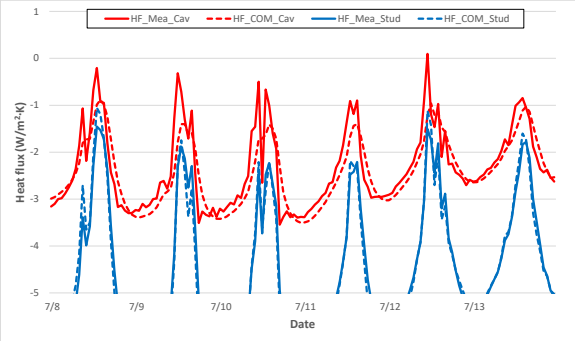

(a) Measured and COMSOL simulated heat fluxes

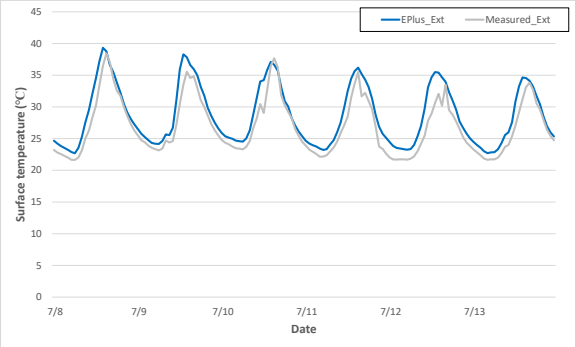

(b) Measured and EnergyPlus simulated exterior surface temperature

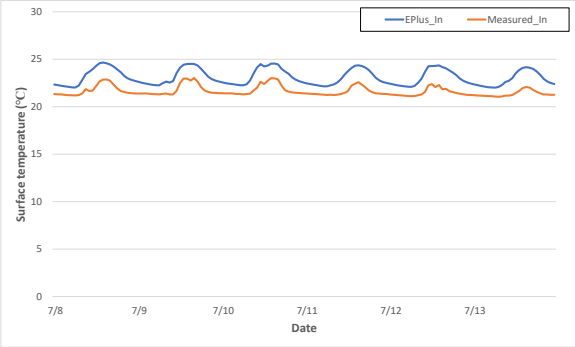

(c) Measured and EnergyPlus simulated interior surface temperature

Figure 9. Measured and simulated results comparison.

4.2.4 Exterior roof evaluation

Figure 10 shows the roof structure and sensor locations. The building has a flat roof with a single-ply membrane on top of tapered polyisocyanurate insulation that sits on a 12.7 mm wood fiberboard sheathing and a corrugated steel metal deck. The plenum space between the roof deck and the dropped ceiling is about 1.5 m. Sets of simulations were carried out to adjust the roof structure, material layers, and properties to make simulation results agree with the measured and simulated heat flux and temperatures. The measured surface temperatures were used as boundary conditions in COMSOL Multiphysics software to fine tune the material properties. The evaluated roof detail is 1D with no thermal bridges, which, therefore, did not require converting the layer properties for EnergyPlus as was needed for the wall case.

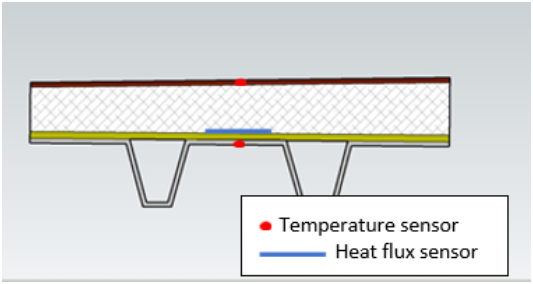

Figure 10. Roof structure and sensor locations.

4.2.5 Exterior roof development

First, we took the material properties from the literature for the originally selected roof structure. The initial simulations resulted in a vastly different performance than was measured. In the series of simulations, we adjusted the thermal conductivity of the polyisocyanurate insulation layer from the assumed 0.024 W/m·K to 0.027 W/m·K to better match the measured and simulated heat fluxes. When comparing EnergyPlus simulation results with the measured exterior surface temperature, we adjusted the solar absorptivity of the exterior surface to 0.9 to improve the agreement. The simulated interior surface temperature was initially very close to the plenum air temperature. We found that the convection heat transfer model “ceiling diffuser” created a high convection heat transfer coefficient on the surface, forcing

the surface temperature to stay close to the air temperature. Choosing "TARP" as the convection heat transfer coefficient model lowered the coefficient radically and increased the surface temperature, providing a close match to the measured temperatures. Finally, the metal deck thermal absorptance was set to 0.1, assuming that the surface is reflective, which helped match the simulated surface temperature to the measured surface temperature. Figure 11 shows the heat flux between the polyisocyanurate insulation and the fiberboard sheathing, as measured and simulated with COMSOL. "Measured" and "COMSOL_HF" in Figure 11 indicate measured heat flux and simulated heat flux from the COMSOL program, respectively. The measured surface temperatures were used as boundary conditions.

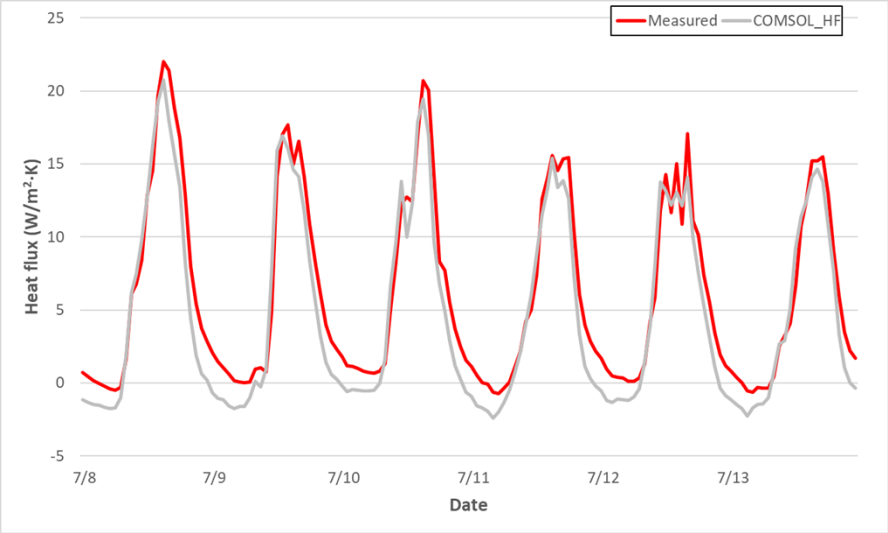

Figure 11. Measured and simulated heat flux result comparison.

The roof structure does not have much thermal mass as it consists mainly of insulation material and thin layers. The transient behavior and peak times agree well. However, the mean bias error in the simulated and measured heat flux of 1.7 W/m^2·K (measured heat flux higher) suggests that there is still some room for adjustment. As described in Figure 11, the measured point of the heat flux is between polyisocyanurate insulation and fiberboard sheathing. The COMSOL program can calculate the heat flux on the measured point, but the EnergyPlus program cannot calculate it since the measured point is neither the inner surface nor the outer surface of the roof. As we confirmed that the calculated heat flux data from the COMSOL program is well matched with the measured data, as shown in Figure 11, we compared the calculated heat flux on the interior surface of the roof from the EnergyPlus program with that from the COMSOL program. Figure 12(a) compares the heat flux on the interior surface of the roof as predicted by COMSOL and EnergyPlus simulation models, and Figure 12(b) and (c) show the exterior and interior surface temperatures as measured and as predicted by the EnergyPlus model. First, EnergyPlus predicts the exterior surface temperature and its peak time quite well. Second, EnergyPlus predicts a lower interior surface temperature than what was measured. "EPlus" and "COMSOL" in Figure 12 indicate simulation results from the EnergyPlus and COMSOL programs. "Old" and "New" in Figure 12 indicate previous and updated simulation results. "HF," "Ext," and "In" in Figure 12 indicate heat flux, exterior surface temperature, and interior surface temperature, respectively. The simulated heat flux and interior and exterior surface temperature data are more similar to measured data than previous simulated data, as shown in Table 5. Both cv(RMSE) and NMBE of the exterior and interior surface temperatures are

improved, as described in Table 4. Even if the simulation model has been improved, it still needs further investigation for the heat flux on the roof.

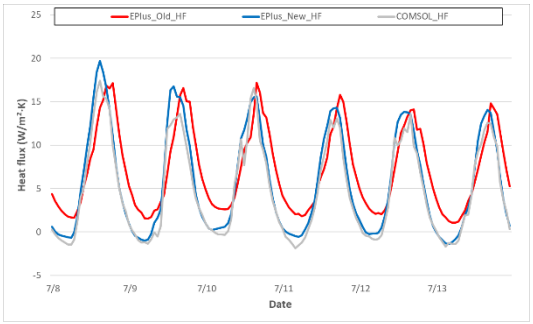

(a) Simulated heat flux data from EnergyPlus and COMSOL

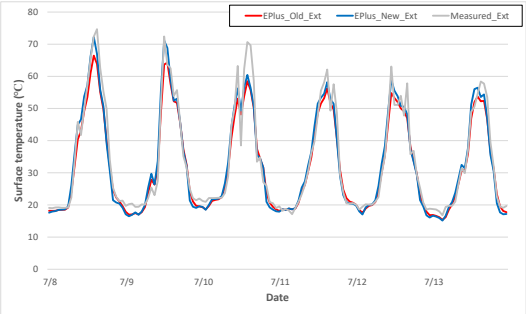

(b) Exterior surface temperature comparison

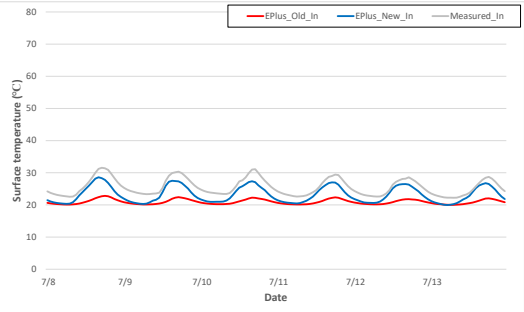

(c) Interior surface temperature comparison

Figure 12. Measured and simulated results comparison.

Table 5. Measured and simulated results comparison.

	Heat flux		**Exterior surface temperature**		**Interior surface temperature**	
	Previous model (%)	Updated model (%)	Previous model (%)	Updated model (%)	Previous model (%)	Updated model (%)
NMBE	48.2	18.0	-4.7	-2.4	-17.9	-9.0
cv(RMSE)	74.4	26.3	11.1	10.6	19.4	9.5

4.3 Window model development

4.3.1 Window model evaluation

For the window model evaluation, we installed the heat flux sensor in the center of the glazing and the temperature sensors in the center and edge of the glazing. To get the glazing properties, we used the "Glass check Pro" device [46], which can measure each layer of glazing including the air gap between the glasses. To get input values of the EnergyPlus simulation program, WINDOW software [47] was used.

4.3.2 Window model development

Energy simulation was performed using a building model that was well-validated for opaque envelope properties and HVAC systems. The detailed window properties, including solar/visible transmittance, reflectance, and thermal conductivity of the layers, were used as input for the EnergyPlus simulation program. The geometric properties of the window, including the frame and divider area, based on the physical measurements of the window components were used as user input for the window properties.

Table 6 shows the updated properties of fenestration. These inputs were used to create a window model in WINDOW software. Then, the model created in WINDOW was exported as an EnergyPlus file.

Table 6. Updated properties of fenestration.

Simulation model	Layer 1 thickness (mm)	Air gap (mm)	Layer 2 thickness (mm)	U-value (W/m²·K)
Previous model	6	15.9	6	2.69
Updated model	3	19	3	2.76

Figure 13 shows the comparison of glass inside and outside surface temperatures for measured and simulation data. In the figure, “Previous” refers to simulated data before the window properties update, and “Updated” refers to the results after the update. We can see from Figure 13(a) and Figure 13(b) that the data from the simulation after update matches more closely to the measured data compared with the data before the window properties update. This difference arising from the window properties update is prominent during the afternoon hours when the temperatures for both inside and outside glass surface temperatures of the previous model are couple of degrees higher than that of the measured and updated model. The results also shows that the surface temperatures of the window closely follow the measured data.

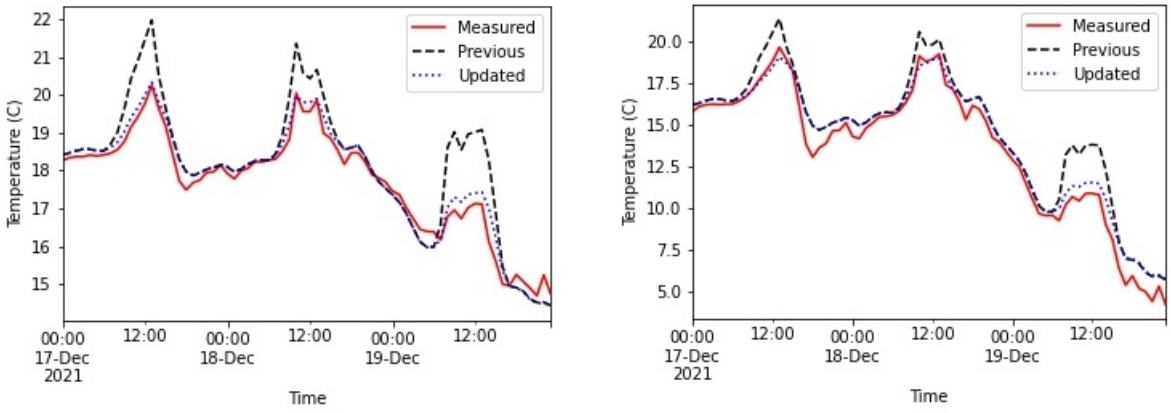

(a) Inside surface temperature

(b) Outside surface temperature

Figure 13. Measured and simulated glass surface temperatures (a) outside (b) inside.

EnergyPlus does not provide the output for the heat flux through the window or frame. Hence, the measured heat flux for the glass and frame were multiplied by their respective area to obtain net heat

transfer through them. For the simulation, the net heat transfer rate of the frame was subtracted from the net heat transfer of the total window to get the net heat transfer rate of the glass. Figure 14 provides the comparison between the measured and simulated net heat transfer rate for the glass. For the glass net heat transfer rate comparison, we used nighttime data only because the heat flux sensors used for the window heat flux measurement are not tailored for conditions when solar radiation is falling into them [48]. Thus, achieving good agreement between the measured and the simulated data during night hours would suffice for validation of window heat transfer.

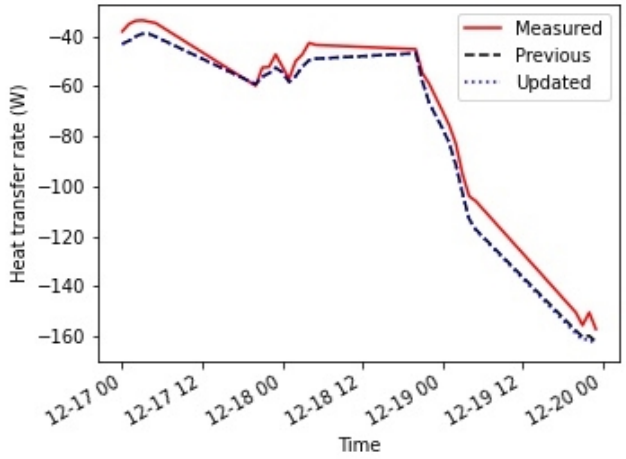

Figure 14. Comparison of the glazing heat transfer rate.

A summary of the difference between measured and simulated data is provided for the updated and the previous simulation model in Table 7. The NMBE and cv(RMSE) for all the variables except "glazing net heat transfer" are calculated for 72 hours of data. For the glazing net heat transfer, only data from 8 p.m. to 5 a.m. was considered to observe the period without any solar irradiation. The table also shows that improvement in NMBE and cv(RMSE) is obtained from use of the updated model.

Table 7. NMBE and cv(RMSE) between measured and simulated data.

Variables	**Previous model**		**Updated model**	
	NMBE (%)	cv(RMSE) (%)	NMBE (%)	cv(RMSE)(%)
Window outside surface temperature	-9	11	-6	8
Window inside surface temperature	-5	7	-3	4
Glazing net heat transfer	-8	-9	-8	-9

The previous results show the importance of using validated input in the energy model and how different inputs can impact the different variables from the simulation engine. For instance, different window construction results in differences in both heat and solar transfer through the window. Also, it can be seen that with validated simulation model input, EnergyPlus can reasonably predict different variables, such as window surface temperatures.

4.4 Infiltration model development

Previous infiltration model [1] is developed by field data in 2019, and we performed another round of the infiltration test for this study. Through the result of the infiltration test, we confirmed that there are the significant changes. In the previous test [1], infiltration rate was around 0.982 m^3/s at 75 Pa (depressurization test), but infiltration rate has been increased as 1.388 m^3/s at 75 Pa (depressurization test). Therefore, for this study, a new infiltration model was developed using the latest measured data. Two different tests were conducted to develop the new infiltration model. One was a blower door test to identify the airflow rate per external wall area, and the other was a tracer-gas test to measure the overall infiltration rate of the building.

Eq. 1 represents the EnergyPlus infiltration model [49].

$$Infiltration = \left(I_{design}\right) \times (F_{sch}) \times \left[\alpha + \beta\left|(T_{zone} - T_{odb})\right| + \gamma\,(W_s) + \delta\,(W_s{}^2)\right] \quad (1)$$

where

I_{design} = Flow per exterior surface area ($m^3/s \cdot m^2$),

F_{sch} = Infiltration schedule,

T_{zone} = Indoor air temperature (°C),

T_{odb} = Outdoor air temperature (°C),

α = Constant coefficient,

β = Coefficient of the indoor and outdoor temperature difference,

γ = Coefficient of wind speed,

δ = Coefficient for the square of wind speed, and

W_s= Wind speed (m/s).

I_{design} can be predicted from the blower door test results. F_{sch} is determined as a value between 0 and 1 to define how much infiltration occurred in total possible infiltration. 1 was used in this study because infiltration always occurred during the test periods. Weighted average indoor temperatures of the conditioned zones were used for T_{zone}. Outdoor air temperature and wind speed data were collected from the weather station on the roof of the FRP building. A, B, C, and D coefficients were fitted with measured infiltration rates. I_{design} can be calculated by (2 [50].

$$I_{design} = \left(\alpha_{bldg} + 1\right) \times I_{75pa} \times \left(\frac{0.5 \times C_s \times \rho \times U_H{}^2}{75}\right)^n \quad (2)$$

where

α_{bldg} = Urban/suburban terrain environment coefficients,

U_H = Reference window speed (m/s),

ρ = Reference air density (kg/m^3),

C_s = Average positive surface pressure coefficient on a wall due to wind effects,

n = Flow exponent, and

I_{75pa} = Air leakage at a pressure differential of 75Pa.

The previous report, which is published by Pacific Northwest National Laboratory, provided some input values to calculate the $I_{design,}$ as shown in Table 8 [50].

Table 8. Input values for I_{design} calculation.

Parameters	Value
α_{bldg}	0.22
U_H	4.47 m/s
ρ	1.18 kg/m^3
C_s	0.1617
n	0.65

Two blower door tests using both pressurization mode and depressurization mode were conducted to determine the building envelope airtightness. During these tests, the HVAC system was off, and all interior doors were open. The airflow rates required to maintain differential pressures of 30 to 75 Pa were measured, and the regression model with flow coefficient and pressure exponent was generated with the measured data (Eq. 3). The blower door test provided the airflow at 50 Pa. To calculate the I_{design}, airflow at 75 Pa is calculated based on the measured data using Eq. 3. Table 9 shows the blower door test schedules and results.

Table 9. Blower door test schedules and results.

Test Date	Mode	Flow Coefficient	Pressure Exponent	Airflow (m^3/s)	
				50 Pa (Measured)	75 Pa (Calculated)
10/27/2021	Pressurization	80.5	0.903	1.300	1.874
12/15/2021	Depressurization	198.8	0.624	1.078	1.388

$$Q = C \times \Delta P^n \ , \tag{3}$$

where

Q = Airflow (m^3/s),

C = Flow coefficient,

ΔP = Pressure differential (Pa), and

n = Pressure exponent,

Four tracer-gas tests were conducted with a multichannel doser and sampler (INNOVA Air Tech Instrument 1303 multipoint sampler and doser), a photoacoustic gas monitor (INNOVA Air Tech Instrument, 1412 photoacoustic field gas monitor), and a tracer-gas (R134a/tetrafluoroethane), which is a nonflammable regrigerant. Six tubes were installed in thermal zones and were connected to the doser and sampler to collect the tracer gas. In this study, we have 10 thermal zones, but we selected 6 thermal zones because of the limitation of the instrument. Table 10 shows the tracer-gas test information, and Figure 15 shows the gas concentration in each floor.

The tracer gas was injected to each room, and the gas concentration (mg/m^3) was measured every 5 minutes. The regression method (Eq. 4) from ASTM Standard E741-00 [51] was used to calculate the infiltration value.

$$\ln(C_{i+t}) = -ACH \times t + \ln(C_i) \quad , \tag{4}$$

where

ACH = Air change per hour (1/h),

C_i, C_{i+t} = Concentration in time i and i+t, and

t = Sample time (h).

Table 10. Tracer-gas test information.

Test ID	Start date and time	Stop date and time	HVAC system status	Test room
T1	2/15/2021 17:04	2/16/2021 7:23	ON	102, 103, 104, 106, 204, 206
T2	4/29/2021 14:30	4/30/2021 4:49	ON	102, 104, 105, 202, 203, 205
T3	5/13/2021 17:19	5/14/2021 7:38	ON	102, 104, 105, 202, 203, 205
T4	7/7/2021 22:01	7/8/2021 12:20	ON	102, 104, 105, 202, 203, 205

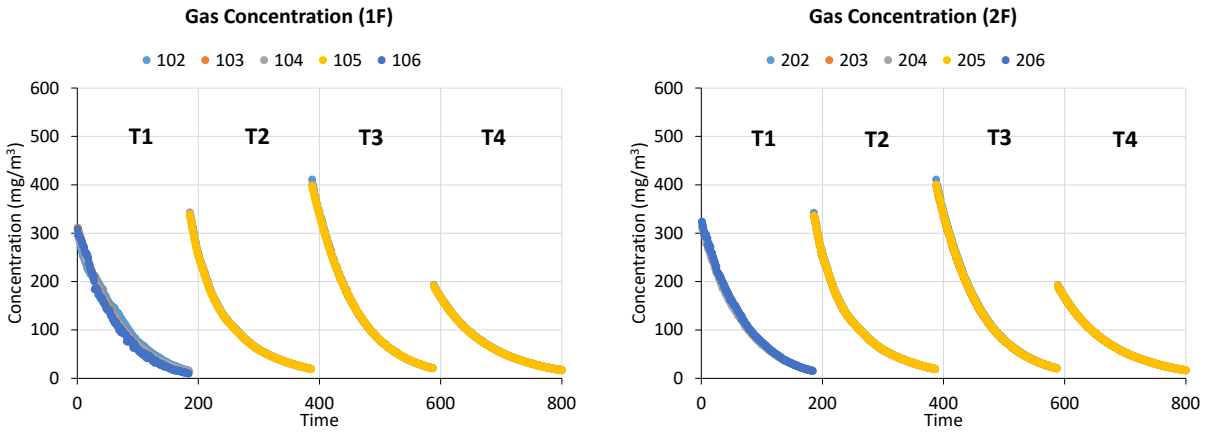

(a) Gas concentration in first floor (b) Gas concentration in second floor

Figure 15. Gas concentration in each floor.

Finally, an infiltration model was developed using the estimated air change per hour (ACH), calculated I_{design} from the tracer-gas and blower door tests, measured indoor and outdoor air temperatures, and measured outdoor temperature.

Figure 16 shows the comparison of infiltration value between actual data and simulation results. "Mea.ACH" and "Calc.ACH" in Figure 16 indicate measured infiltration value and calculated infiltration value using Eq. 1.

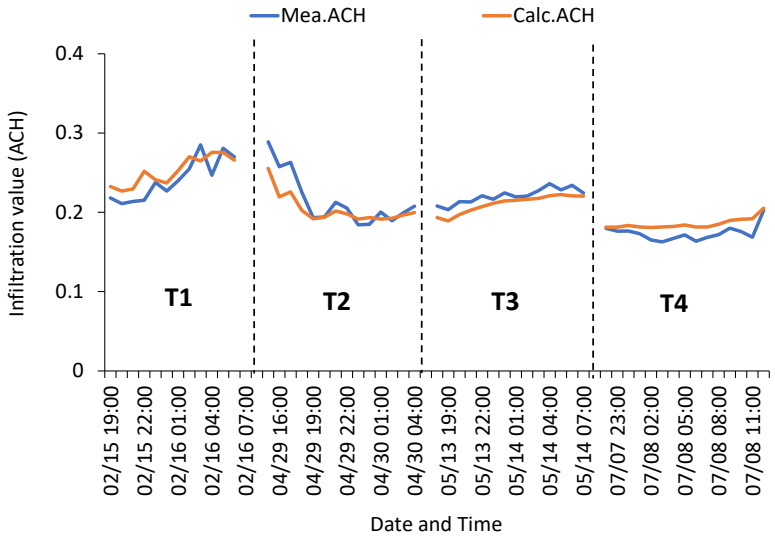

Figure 16. Infiltration comparison.

4.5 RTU cooling performance curve development

The performance curve in building energy simulation has significant impact on the HVAC capacity and energy consumption predictions. In this study, cooling performance curves for EnergyPlus were generated based on the information of cooling system and collected performance data during a field test. In the EnergyPlus simulation program, five different performance curves are required for the RTU [52]:

- Total cooling capacity function of temperature curve (CFT)
- Total cooling capacity function of flow fraction curve (CFF)
- Energy input ratio function of temperature curve (EFT)
- Energy input ratio function of flow fraction curve (EFF)
- Part load fraction correlation curve (PLF)

Eq. 5 through Eq. 11 show how to generate the five cooling performance curves and how they affect cooling energy consumption [52].

$$Power = \dot{Q}_{total,rated} \times (CFT) \times (CFF) \times \left(\frac{1}{COP_{rated}}\right) \times (EFT) \times (EFF) \times \left(\frac{PLR}{PLF}\right) , \quad (5)$$

$$CFT = c_{CFT,1} + c_{CFT,2} \times WT + c_{CFT,3} \times WT^2 + c_{CFT,4} \times DT + c_{CFT,5} \times DT^2 + c_{CFT,6} \times WT \times L \quad (6)$$

$$CFF = c_{CFF,1} + c_{CFF,2} \times ff + c_{CFF,3} \times ff^2 , \quad (7)$$

$$EFT = c_{EFT,1} + c_{EFT,2} \times WT + c_{EFT,3} \times WT^2 + c_{EFT,4} \times DT + c_{EFT,5} \times DT^2 + c_{EFT,6} \times WT \times DT , \quad (8)$$

$$EFF = c_{EFF,1} + c_{EFF,2} \times ff + c_{EFF,3} \times ff^2 , \quad (9)$$

$$PLF = c_{PLF,1} + c_{PLF,2} \times PLR \text{ , and} \quad (10)$$

$$PLR = \frac{actual\ sensible\ cooling\ load}{steady - state\ sensible\ cooling\ load} , \quad (11)$$

where

Power = Electric energy consumption of the cooling system (Wh),

$\dot{Q}_{total,rated}$ = Rated total cooling capacity (W),

COP_{rated} = Coefficient of performance at rated conditions,

PLR = Part load ratio (%),

WT = Entering web-bulb temperature (°C),

DT = Dry-bulb temperature seen by condenser (°C),

ff = Fraction of the full load flow (%), and

c = Coefficient for each curve.

To generate the cooling performance curves, the web-bulb temperature entering a cooling coil, airflow rate in the duct, and dry-bulb temperature seen at the condenser were measured at 1-hour intervals during the cooling season test. At the same time, the rated capacity of the cooling coil, rated coefficient of performance of the cooling coil, and airflow rate were found from the HVAC system specifications. With the measured and rated values, performance curves were generated.

Figure 17(a) shows the comparison of measured and predicted available capacities from the generated curve coefficient values. The predicted available capacity is well matched well with available capacity which is calculated by the measured dataset, during the test season; NMBE and cv(RMSE) were -0.1% and 7.1%, respectively. Figure 17(b) shows cooling energy consumption comparison between measured and predicted. It shows that the measured and predicted cooling energy consumption are in good agreement. The NMBE and cv(RMSE) for cooling energy consumption were -0.2% and 6.1%, respectively.

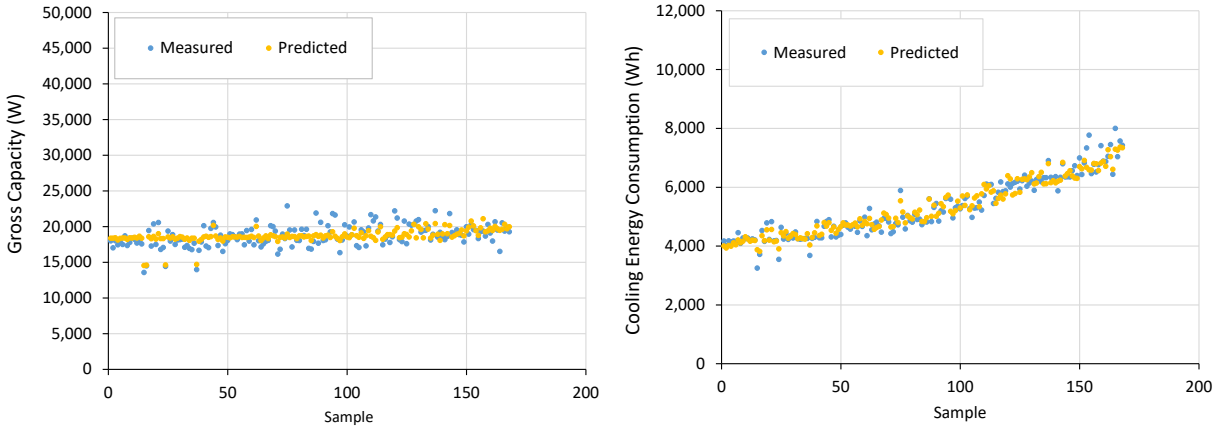

(a) Comparison of measured and predicted available capacity

(b) Comparison of measured and predicted cooling energy consumption

Figure 17. Comparison of measured and predicted available capacity and cooling energy consumption by performance curves.

The available capacity affects the humidity ratio, as shown in Eq. 12 [52]. According to the equation, the available cooling capacity and air enthalpy at the apparatus dew point condition are inversely proportional. If available cooling capacity is oversized, air enthalpy at the apparatus dew point condition will be decreased. In general, the lower enthalpy of air at the apparatus dew point condition results in the lower effective coil surface temperature. The lower the effective cooling coil surface temperature, the more humidity can be removed. For this reason, the performance curve is important not only for energy consumption but also for humidity ratio.

$$h_{ADP} = h_{in} - \frac{(Q_{total}/m)}{1 - BF} \quad , \tag{12}$$

where

h_{ADP} = Enthalpy of air at the apparatus dew point condition (J/kg),

h_{in} = Enthalpy of air entering the cooling coil (J/kg),

Q_{total} = Available cooling capacity (W),

m = air mass flow rate (kg/s), and

BF = bypass factor.

5. Results

To understand the impact of the simulation model input parameter validation on building indoor thermal conditions and energy consumption, we compare the simulation results from both the previous model and the updated model to measured data. The analysis period is from July 7, 2021, to July 14, 2021, when the experimental study was conducted. Simulation input for the previous model came from the previous study

[1], and input for the updated model came from the updated BEM from this study (e.g., building geometry model, infiltration model, and cooling performance curve). “Previous,” “Updated,” and “Measured” in Figure 18 and Table 11 indicate simulation results from the previous model, simulation results from the updated model, and measured data, respectively.

5.1 Indoor thermal condition

As described in Figure 1, one of the limitations in the previous paper [1] was indoor air temperature differences between simulation results and measured data. Figure 18 compares the weighted indoor air temperature and relative humidity between simulation results and measured data. Since the test building has 10 conditioned zones, to compare the indoor air temperature and relative humidity we used the weighted average indoor air temperature and relative humidity data. As shown in Table 11, both the NMBE and cv(RMSE) of the weighted indoor air temperature and weighted indoor relative humidity were improved through the improved inputs to the simulation model. Notably, the weighted indoor air relative humidity improved significantly mainly due to the improved performance curve. The indoor air relative humidity is affected by the outdoor condition and supply air relative humidity. For the outdoor condition, we updated the infiltration model through the blower door test and tracer-gas test, as described in Section 4.4. The supply air relative humidity is discussed in Section 5.2. We confirmed that the indoor condition is improved through the simulation input parameter validation from this study.

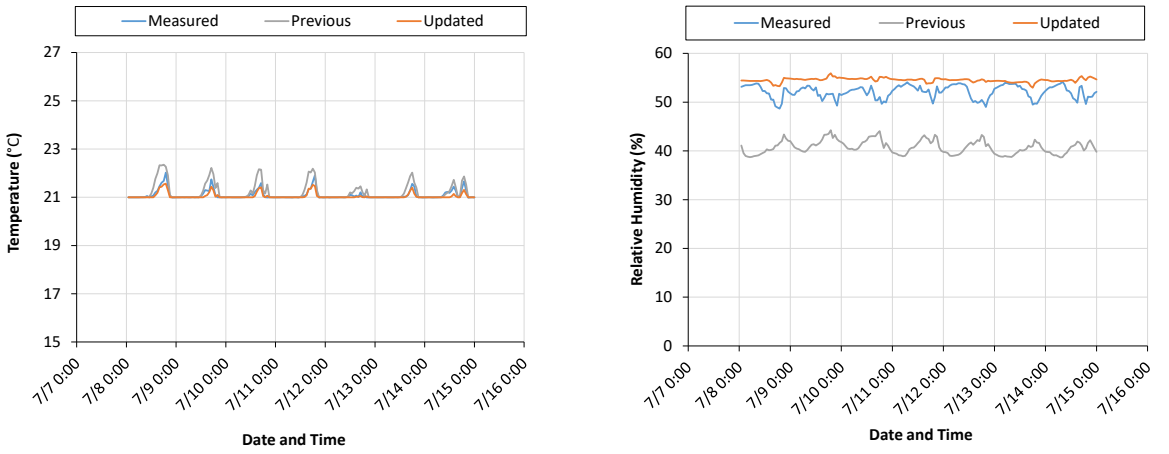

(a) Weighted average indoor air temperature

(b) Weighted average indoor air relative humidity

Figure 18. Weighted average indoor air temperature and relative humidity.

Table 11. NMBE and cv(RMSE) values of indoor air temperature and relative humidity.

	Weighted average indoor air temperature		**Weighted average indoor air relative humidity**	
	Previous model (%)	**Updated model (%)**	**Previous model (%)**	**Updated model (%)**
NMBE	-0.6	0.2	21.8	-4.6
cv(RMSE)	1.1	0.5	22.3	5.3

5.2 Supply and return air

Figure 19 shows the comparing supply and return air temperatures and relative humidity between simulation results and measured data. Supply air temperature means supply air temperature from the RTU and return air temperature means return air from the conditioned zones to the RTU. Table 12 shows the value of NMBE and cv(RMSE) for supply and return air temperature and relative humidity. “SAT,” “SARH,” “RAT,” and “RARH” in Table 12 indicate supply air temperature, supply air relative humidity, return air temperature, and return air relative humidity, respectively.

Since the supply air temperature is followed by the supply air setpoint temperature, there is no difference between the previous model results and the updated model results. The supply air relative humidity improved significantly because of the validated cooling performance curve, especially the capacity curve. As described in Section 4.5, the previous RTU capacity curve was slightly exaggerated. The oversized available cooling capacity lowers the enthalpy of air at the apparatus dew point condition and allows more humidity to be removed through the lower effective cooling coil surface temperature. Therefore, the supply air relative humidity of the previous model is lower than that of the updated model and measured data. Because one of the test settings used for the HVAC operation was 100% return air, the return air relative humidity is directly affected by the indoor air relative humidity. Return air relative humidity was improved because indoor air relative humidity was improved. Since supply and return air temperature and supply and return air relative humidity of the updated model were well-matched with measured data, it can be said that the updated model operates more similarly to the test building than the previous model not only for the sensible cooling but also from the latent cooling perspective.

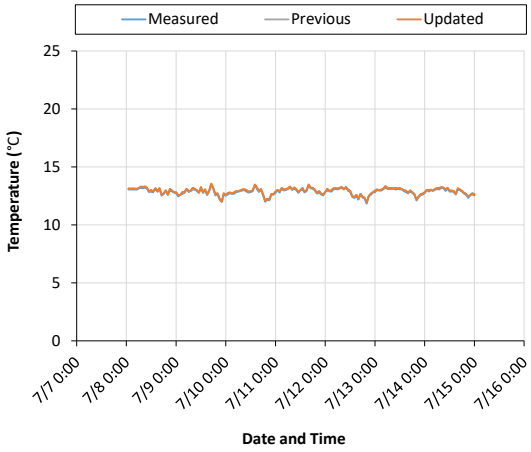

(a) Supply air temperature

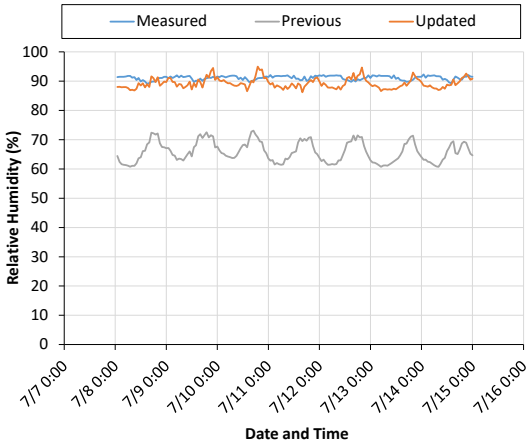

(b) Supply air relative humidity

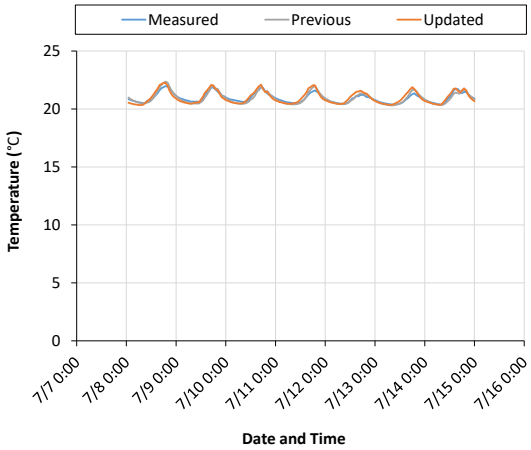

(c) Return air temperature

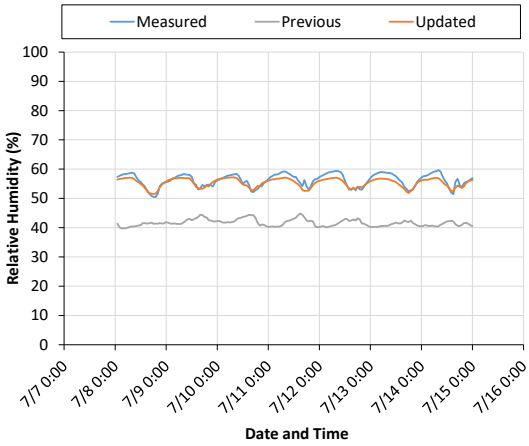

(d) Return air relative humidity

Figure 19. Supply and return air temperature and relative humidity.

Table 12. Comparison supply and return air between simulation results and measured data.

	SAT		SARH		RAT		RARH	
	Previous model (%)	**Updated model (%)**	**Previous model (%)**	**Updated model (%)**	**Previous model (%)**	**Updated model (%)**	**Previous model (%)**	**Updated model (%)**
NMBE	-0.6	-0.6	27.8	2.1	0.1	-0.2	25.9	1.6
cv(RMSE)	-0.7	-0.7	28.1	3.0	0.7	1.1	26.4	2.4

5.3 Energy use

Figure 20 shows the comparison of the supply airflow rate and fan energy consumption between field data and simulation results of both the previous model and the updated model. To minimize energy consumption of the VAV boxes, each VAV box requests minimum airflow through the damper control [53]. Since the sum of airflow of all VAV boxes is the same as airflow from the RTU, supply airflow from the RTU is constant. Fan energy consumption is also fixed because of the fixed supply airflow from the RTU.

Figure 21 compares the total delivered cooling energy and cooling energy consumption between field data and simulation results of both the previous model and the updated model. Total delivered cooling energy is calculated by the sum of sensible cooling energy and latent cooling energy. This means that not only temperature but also humidity is important for calculating the total delivered cooling energy. The test setting in this study has no outdoor air intake for HVAC system operation, which means return air is used 100% for HVAC system operation. Because 100% return air is used for HVAC system operation, indoor air relative humidity is important, which is why we compare the indoor air relative humidity in the previous section. As seen in Section 5.2, both simulated indoor air temperature and relative humidity in

the updated model are well matched with field data, and the total delivered cooling energy is also well matched.

Table 13 and Table 14 show the comparison of NMBE and cv(RMSE) values of between the previous model and the updated model. Through these, we confirm that the simulation model input parameter validation affected not only indoor thermal conditions but also the HVAC system-level condition.

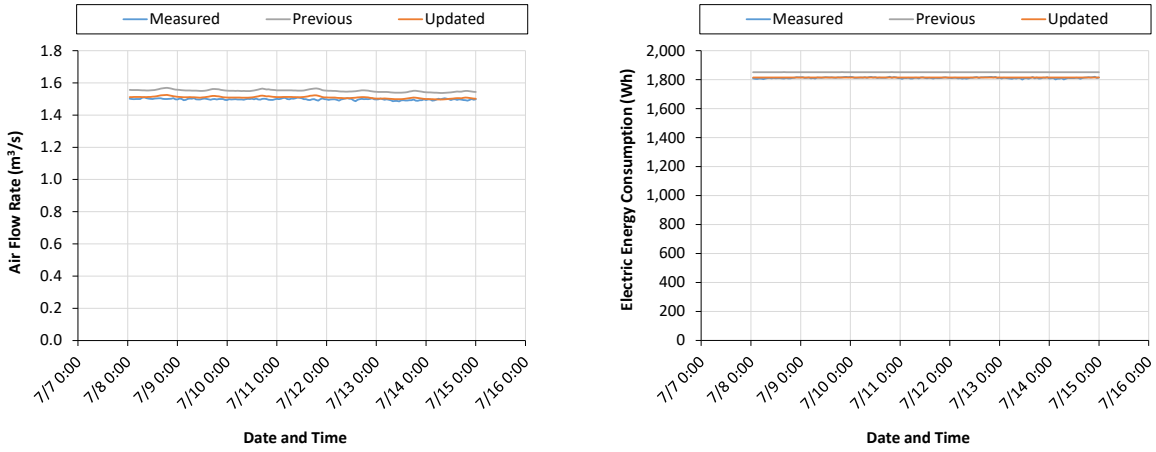

(a) Supply fan airflow rate

(b) Supply fan energy consumption

Figure 20. Supply fan airflow rate and energy consumption.

Table 13. NMBE and cv(RMSE) values of supply airflow rate and fan energy consumption.

	Supply fan air flow rate		**Supply fan energy consumption**	
	Previous model (%)	Updated model (%)	Previous model (%)	Updated model (%)
NMBE	-3.6	-0.8	-2.2	-0.2
cv(RMSE)	3.6	0.9	2.2	0.3

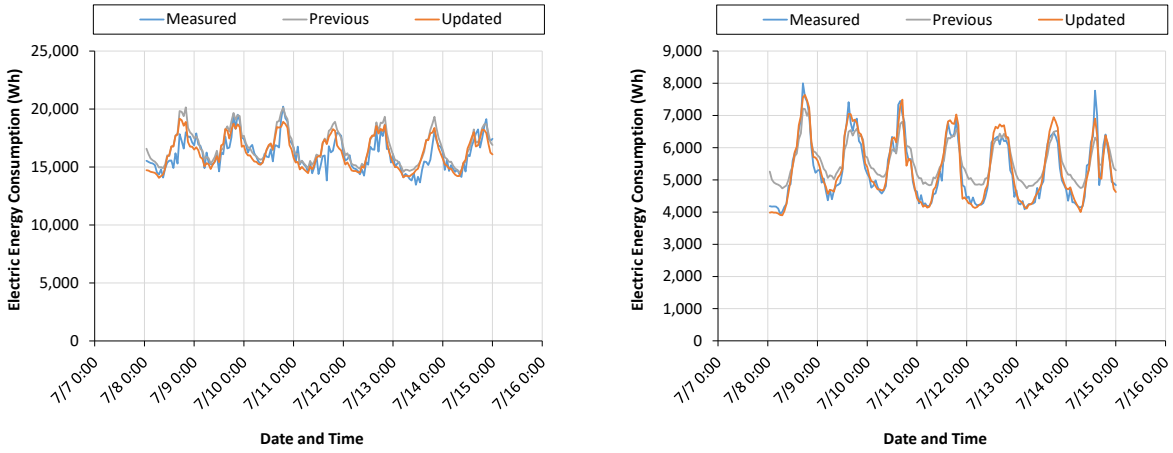

(a) Total delivered cooling energy

(b) Total cooling energy consumption

Figure 21. RTU delivered cooling energy and electric energy consumption.

Table 14. NMBE and cv(RMSE) values of delivered cooling energy and cooling electric energy consumption.

	Total delivered cooling energy		**Cooling energy consumption**	
	Previous model (%)	**Updated model (%)**	**Previous model (%)**	**Updated model (%)**
NMBE	-4.0	-0.9	-4.9	-1.0
cv(RMSE)	6.0	5.6	9.6	4.7

Figure 22 shows the electric energy consumption of the VAV boxes of both the previous model and the updated model. The test building has 10 conditioned zones, and each zone has 1 VAV box. This means the value in Figure 22 is the sum of the electric energy consumption of the 10 VAV boxes. The NMBE and cv(RMSE) for electric energy consumption of the VAV boxes in the previous model were 12.4% and 19.6%, respectively. The NMBE and cv(RMSE) for electric energy consumption of the VAV boxes in the updated model were 5.2% and 10.1%, respectively.

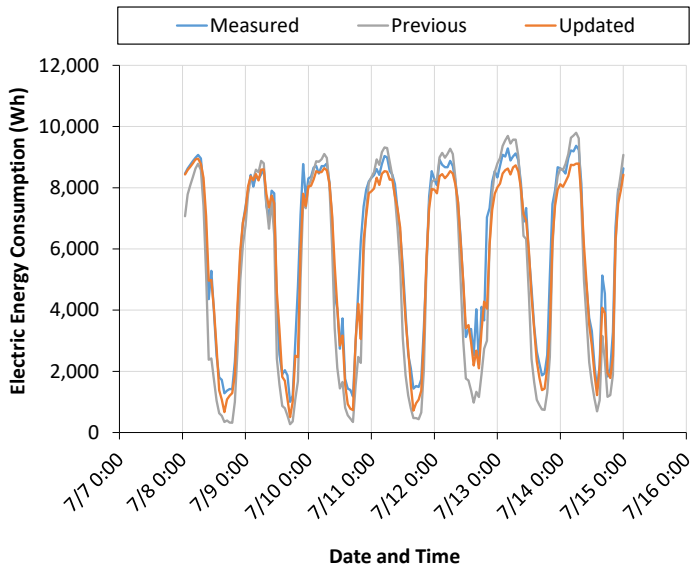

Figure 22. Total VAV reheating energy consumption.

Figure 23 shows the total HVAC electric energy consumption comparison between field data and simulation results of both the previous model and the updated model. Heating is from VAV boxes, and cooling is from the DX cooling coil in the RTU. In terms of the fan energy consumption and cooling energy consumption, the simulation result of the updated model is almost the same as the measured data, with a difference of only 1 kWh. When summing the cooling energy consumption and fan energy consumption, the simulation result of the updated model is the same as the measured data, with a difference of only 9 kWh, which means a difference of 0.01%. The NMBE and cv(RMSE) of the total HVAC energy consumption in the previous model were 3.4% and 9.6%, respectively. With the improved simulation model inputs, the NMBE and cv(RMSE) were improved by 2.0% and 4.3%, respectively.

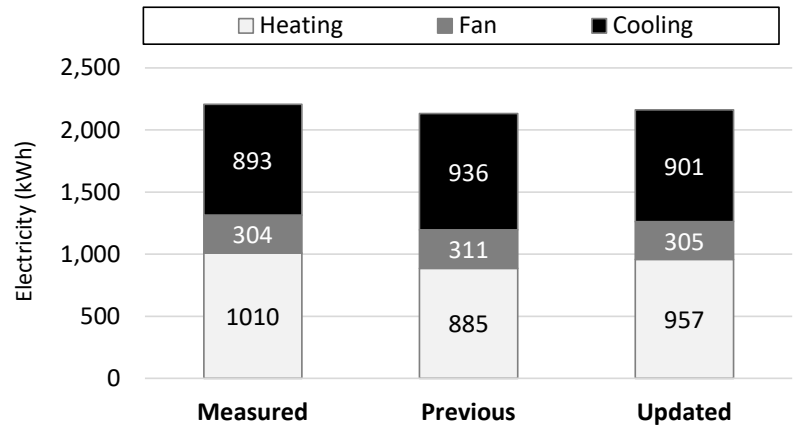

Figure 23. Total HVAC energy consumption.

6. Conclusion and future study

This paper has presented the importance of component-level empirical validation efforts for building energy model validation. The validation process and results have demonstrated the criticality of whole-building energy model validation with component-level empirical validations. While traditional validation methods often rely solely on comparing whole-building energy use, this approach, while effective in energy use, falls short in guaranteeing the model's accuracy with respect to other critical aspects, such as the building envelope, building behavior, and indoor environmental conditions.

- In this study, we thoroughly examined actual building components and developed energy models based on real building data. In terms of the building envelope (exterior walls and roofs), the simulation models are often simplified due to the complexity of the actual structure. To address this issue, we used detailed multiphysics simulations (COMSOL) to validate the simulation input parameter of exterior wall and roof models.
- For the exterior wall, after simulation input parameter validation, we found that the NMBE for exterior and interior surface temperatures decreased to 6.8% and 6.5%, respectively. Additionally, the cv(RMSE) for exterior and interior surface temperatures decreased to 7.1% and 8.0%, respectively. For the exterior roof, the NMBE values for heat flux, exterior surface temperature, and interior surface temperature decreased by 30.2%, 2.3%, and 8.9%, respectively. Likewise, the cv(RMSE) values for heat flux, exterior surface temperature, and interior surface temperature decreased by 48%, 0.5%, and 9.9%, respectively. Overall, the decrease in both NMBE and cv(RMSE) indicates that the simulation models for the exterior wall and roof closely match the actual building conditions after our efforts to validate the simulation input parameters.
- Similar to exterior walls and roofs, windows are often simplified in simulations, overlooking critical details like glazing and frames. However, we took precise measurements of each glazing and frame, along with indoor and outdoor temperatures and heat transfer, to evaluate how closely our simulated windows matched the actual building's thermal properties. After validating the simulation input parameters, we achieved a reduction of 3% in the NMBE for outside surface temperature and 2% for inside surface temperature. Additionally, the cv(RMSE) decreased by 3% for exterior surface temperature, and 3% for interior surface temperature. In summary, the decrease in both NMBE and cv(RMSE) indicates that the simulation model for exterior windows closely resembles the actual building conditions after our efforts to validate the simulation input parameters.
- Regarding infiltration, we conducted blower door and tracer gas tests under various weather conditions. This is because infiltration is influenced by various factors, including HVAC, wind speed, and indoor/outdoor temperature variations.
- Regarding the performance curve, our investigation unveiled a significant impact of cooling capacity not only on cooling energy consumption but also on indoor humidity levels within the building. Our study discovered that available capacity has an influence on humidity ratios. Consequently, to validate simulation input parameters, it is imperative to develop performance curves utilizing actual datasets. To ensure accuracy, we developed performance curves using measured dataset, and our predicted available capacity closely matched the measured dataset, with an NMBE of -0.1% and a cv(RMSE) of 7.1%. To gain a deeper understanding of how each

curve affects simulation outcomes, a more comprehensive examination is necessary. This is particularly crucial because the cooling system requires five performance curves.

- Validating simulation input parameters results in significant enhancements in simulation result accuracy. Notably, both NMBE and cv(RMSE) values are reduced by 0.5% for indoor air temperature and by 17% for indoor air relative humidity compared to the previous model. Moreover, at the system level, both NMBE and cv(RMSE) values exhibit reductions of 2% for fan energy consumption and 4% for cooling energy consumption when compared to the previous model.

In summary, this study emphasizes the importance of simulation input parameter validation with actual data. We also explored and shared strategies for addressing the complexities and limitations associated with aligning simulation models as closely as possible with actual building. These efforts are important for improving the accuracy and reliability of building energy simulations.

In our forthcoming research, we will diligently address any lingering inconsistencies in specific areas that demand further investigation and improvement. Our approach will focus on enhancing the accuracy of the zone model by conducting zone-specific air exchange tests using differential pressure sensors and the CONTAM program. Additionally, our future investigations will explore models related to inter-zone air mixing, with the aim of enhancing the model's precision. Furthermore, we have plans to assess the model's performance under various operational scenarios, including conditions such as night setback and free-floating situations, across different seasons. We will also ensure the verification of simulation input parameters not only within the EnergyPlus simulation program but also across other simulation programs. This thorough empirical validation strategy is designed to ensure the model's accuracy and create a valuable empirical validation dataset that can be beneficial to the wider research community.

Acknowledgement

This material is based upon work supported by the US Department of Energy's (DOE's) Office of Science and Building Technologies Office (BTO). This research used resources of Oak Ridge National Laboratory's Building Technologies Research and Integration Center, which is a DOE Office of Science User Facility. This work was funded by fieldwork proposal CEBT105 under BTO activities BT0302000 and BT0305000. This manuscript has been authored by UT-Battelle LLC under contract DEAC05-00OR22725 with DOE. The US government retains and the publisher, by accepting the article for publication, acknowledges that the US government retains a nonexclusive, paid-up, irrevocable, worldwide license to publish or reproduce the published form of this manuscript, or allow others to do so, for US government purposes. The authors wish to acknowledge for Tony Gehl's contributions to field test. Finally, we thank ASHRAE SSPC140 technical committee for their valuable feedback, and Amir Roth of US Department of Energy, Building Technologies Office for his generous support for this project.

References

[1] Im P, Joe J, Bae Y, New JR. Empirical validation of building energy modeling for multi-zone commercial buildings in cooling season. Appl Energy 2020;261:114374.

[2] Moreci E, Ciulla G, Brano VL. Annual Heating Energy Requirements of Office Buildings in a European Climate. Sustain Cities Soc. 2016;20:81–95.

[3] Ahn B, Jang C, Leigh S, Jeong H. Analysis of the Effect of Artificial Lighting on Heating and Cooling Energy in Commercial Buildings. Energy Procedia 2014;61:928–32.

[4] Baloch AA, Shaikh PH, Shaikh F, Leghari ZH, Mirjat NH, Uqaili MA. Simulation tools application for artificial lighting in buildings. Renew Sustain Energy Rev 2018;82:3007-26.

[5] Pang Z, Chen Y, O'Neill Z, Cheng H, Dong B. Nationwide HVAC energy-saving potential quantification for office buildings with occupant-centric controls in various climates. Appl Energy 2020;279:115727.

[6] Afroz Z, Shafiullah GM, Urmee T, Higgins G. Modeling techniques used in building HVAC control systems: A review. Renew Sustain Energy Rev 2018;83:64-84.

[7] Cascia EL, Ma Z, Borelli D, Schenone C. Residential Building Retrofit through Numerical Simulation: A Case Study. Energy Procedia 2017;111:91–100.

[8] Deb C, Schlueter A. Review of data-driven energy modelling techniques for building retrofit. Renew Sustain Energy Rev 2021;144:110990.

[9] Zhang R, Hong T. Modeling of HVAC operational faults in building performance simulation. Appl Energy 2017;202:178–88.

[10] Zhao Y, Li T, Zhang X, Zhang C. Artificial intelligence-based fault detection and diagnosis methods for building energy systems: Advantages, challenges and the future. Renew Sustain Energy Rev 2019;109:85-101.

[11] Ekström T, Burke S, Wiktorsson M, Hassanie S, Harderup L, Arfvidsson J. Evaluating the impact of data quality on the accuracy of the predicted energy performance for a fixed building design using probabilistic energy performance simulations and uncertainty analysis. Energy Build 2021;249:111205.

[12] Deb C, Zhang F, Yang J, Lee SE, Shah KW. A review on time series forecasting techniques for building energy consumption. Renew Sustain Energy Rev 2017;74:902-24.

[13] Ahmad M, Culp CH. Uncalibrated Building Energy Simulation Modeling Results. HVAC&R Res 2006;12:1141-55.

[14] Coakley D, Raftery P, Keane M. A review of methods to match building energy simulation models to measured data. Renew Sustain Energy Rev 2014;37:123-41.

[15] U.S. Department of Energy. ASHRAE Standard 140 Maintenance and Development, https://www.energy.gov/eere/buildings/ashrae-standard-140-maintenance-and-development; 2023 [accessed 02 Feburary 2023].

[16] American Society of Heating, Refrigerating and Air-Conditioning Engineers. ASHRAE standard 140-2014. Standard Method of Test for the Evaluation of Building Energy Analysis Computer Programs. Atlanta: American Society of Heating, Refrigerating, and Air Conditioning Engineers 2014.

[17] Judkoff R, Wortman D, O'Doherty B, Burch J. A Methodology for Validating Building Energy Analysis Simulation. Technical Report; National Renewable Energy Laboratory (NREL): Golden, CO, USA, U.S. Department of Energy, https://www.nrel.gov/docs/fy08osti/42059.pdf; 2008.

[18] Judkoff R, Neymark J. Model validation and testing: The methodological foundation of ASHRAE Standard 140. ASHRAE Transact 2006;112:367–76.

[19] Loutzenhiser PG, Manz H, Strachan PA, Felsmann C, Frank T, Maxwell GM, Oelhafen P. An Empirical Validation of Modeling Solar Gains through a Glazing Unit Using Building Energy Simulation Programs. HVAC&R Res 2006;12:1097–116.

[20] Loutzenhiser PG, Manz H, Carl S, Simmler H, Maxwell GM. Empirical validations of solar gain models for a glazing unit with exterior and interior blind assemblies. Energy Build 2008;40:330-40.

[21] Loutzenhiser PG, Manz H, Felsmann C, Strachan PA, Maxwell GM. An empirical validation of modeling solar gain through a glazing unit with external and internal shading screens. Appl Therm Eng 2007;27:528-38.

[22] Wetter M, Wangda Z, Nouidui TS, Pang X. Modelica Buildings Library. J Build Perform Simul 2014;7:253–70.

[23] Nouidui TS, Wetter M, Zuo W. Validation of the Window Model of the Modelica Buildings Library. Technical report, Lawrence Berkeley National Laboratory (LBNL), Berkeley, CA, USA, https://escholarship.org/uc/item/0b5624k9; 2012.

[24] Lucchino EC, Gelesz A, Skeie K, Gennaro G, Reith A, Serra V, Goia F. Modelling double skin façades (DSFs) in whole-building energy simulation tools: Validation and inter-software comparison of a mechanically ventilated single-story DSF. Build Environ 2021;199:107906.

[25] Mateus NM, Pinto A, Graca GC. Validation of EnergyPlus thermal simulation of a double skin naturallyand mechanically ventilated test cell. Energy Build 2014;75:511-22.

[26] Kalyanova O, Heiselberg P, Felsmann C, Poirazis H, Strachan P, Wijsman A. An empirical validation of building simulation software for modeling of double-skin facade (DSF). In: Proceedings of 11th International Conference on Building Simulation. 2009.

[27] Kuznik F, Virgone J, Johannes K. Development and validation of a new TRNSYS type for the simulation of external building walls containing PCM. Energy Build 2010;42:1004-9.

[28] Buonomano A and Guarino F. The impact of thermophysical properties and hysteresis effects on the energy performance simulation of PCM wallboards: Experimental studies, modelling, and validation. Renew Sustain Energy Rev 2020;126:109807.

[29] Herrando M, Coca-Ortegon A, Guedea I, Fueyo N. Experimental validation of a solar system based on hybrid photovoltaic-thermal collectors and a reversible heat pump for the energy provision in non-residential buildings. Renew Sustain Energy Rev 2023;178:113233.

[30] Cattarin G, Pagliano L, Causone F, Kindinis A. Empirical and Comparative Validation of an Original Model to Simulate the Thermal Behaviour of Outdoor Test Cells. Energy Build 2018;158:1711–23.

[31] Eguía-Oller P, Martínez-Mariño S, Granada-Álvarez E, Febrero-Garrido L. Empirical validation of a multizone building model coupled with an air flow network under complex realistic situations. Energy Build 2021;249:111197.

[32] Nageler P, Schweiger G, Pichler M, Brandl D, Mach T, Heimrath R, Schranzhofer H, Hochenauer C. Validation of Dynamic Building Energy Simulation Tools Based on a Real Test-Box with Thermally Activated Building Systems (TABS). Energy Build 2018;168:42–55.

[33] Barone G, Buonomano A, Forzano C, Palombo A. Building Energy Performance Analysis: An Experimental Validationof an In-House Dynamic Simulation Tool through a Real Test Room. Energies 2019;12:4107.

[34] Strachan P, Svehla K , Heusler I, Kersken M. Whole model empirical validation on a full-scale building. J Build Perform Simul 2016;9:331-50.

[35] Campbell Scientific. HC2S3-LTemperature and Relative Humidity Probe, https://www.campbellsci.com/hc2s3; 2023 [accessed 03 Feburary 2023].

[36] Continental Control Systems, LLC. WNC Series WattNode BACnet – Info, https://ctlsys.com/support/wattnode-bacnet/; 2023 [accessed 03 Feburary 2023].

[37] Omega. Configurable, High Accuracy Pressure Transducers, https://www.omega.com/en-us/pressure-measurement/pressure-transducers/p/PX409-Series; 2023 [accessed 03 Feburary 2023].

[38] Air Monitor. VELTRON DPT 2500-plus Transmitter, https://www.airmonitor.com/hvac/product/veltron-dpt-2500-plus-transmitter/; 2023 [accessed 03 Feburary 2023].

[39] Hukseflux USA. FHF03 Sensor specifications, https://huksefluxusa.com/shop/heat-flux-products/heat-flux-sensors/fhf03-foil-heat-flux-sensor/; 2023 [accessed 03 Feburary 2023].

[40] Yoon Y, Jung S, Im P. Datasets of a Multizone Office Building under Different HVAC System Operation Scenarios. Scientific Data 2020; 9 : 1-11.

[41] Im P, Jung S, Yoon Y. Datasets of a Multizone Office Building under Different HVAC System Operation Scenarios. Figshare 2022, https://doi.org/10.6084/m9.figshare.20520438.v3 [accessed 14 September 2023].

[42] American Society of Heating, Refrigerating and Air-Conditioning Engineers. ASHRAE Guideline 14-2014, 2014.

[43] Federal Energy Management Program. M&V Guidelines: Measurement and Verification for Performance-Based Contracts Version 4.0, 2015.

[44] International Performance Measurement & Verification Protocol International Performance Measurement and Verification Protocol: Concepts and Options for Determining Energy and Water Savings; Technical Report; Efficiency Valuation Organization, Washington, DC, USA; 2012.

[45] COMSOL Inc. COMSOL, http://www.comsol.com; 2023 [accessed 03 Feburary 2023].

[46] Electronic Design to Market. Glass Check PRO device manual, https://www.edtm.com/images/stories/pdf/manuals/GC3001-manual_web.pdf; 2023 [accessed 03 Feburary 2023].

[47] Lawrence Berkeley National Laboratory. WINDOW Technical Documentation, https://windows.lbl.gov/tools/window/documentation; 2020 [accessed 03 Feburary 2023].

[48] Hukseflux. User manual HFP01 & HFP03 heat flux plate / heat flux sensor, https://www.hukseflux.com/uploads/product-documents/HFP01_HFP03_manual_v2123.pdf; 2021 [accessed 03 Feburary 2023].

[49] U.S. Department of Energy. EnergyPlus version 9.4.0 documentation, Input Output Reference. 2020.

[50] Gowri K, Winiarski D, Jarnagin R. Infiltration Modeling Guidelines for Commercial Building Energy Analysis. Technical Report, Parcific Northwest Laboratory (PNNL), Richland, WA, USA, https://www.pnnl.gov/main/publications/external/technical_reports/PNNL-18898.pdf; 2009.

[51] ASTM International. Standard E741-00 - Standard Test Method for Determining Air Change in a Single Zone by Means of a Tracer Gas Dilution. West Conshohocken, PA: ASTM International. 2006.

[52] U.S. Department of Energy. EnergyPlus version 9.4.0 documentation, Engineering Reference. 2020.

[53] Wang L, Mathew P, Pang X. Uncertainties in Energy Consumption Introduced by Building Operations and Weather for a Medium-Size Office Building. Technical Report, Lawrence Berkeley

National Laboratory (LBNL), Berkeley, CA, USA, https://www.osti.gov/servlets/purl/1172957; 2012 [accessed 03 Feburary 2023].